RSC Advances

PAPER

View Article Online
View Journal | View Issue

Cite this: *RSC Adv.*, 2024, **14**, 20799

Hydrazone-functionalized nanoscale covalent organic frameworks as a nanocarrier for pH-responsive drug delivery enhanced anticancer activity†

Datian Fu,‡[a] LiLi Zhong,‡[b] Jin Xu,[c] Anwei Mo[d] and Min Yang *[e]

Nanoscale covalent organic frameworks (NCOFs) as emerging drug-delivery nanocarriers have received much attention in biomedicine in recent years. However, there are few reports on the application of pH-responsive NCOFs for drug delivery nanosystems. In this work, hydrazone-decorated NCOFs as pH-triggered molecular switches are designed for efficient cancer therapy. These functionalized NCOFs with hydrazone groups on the channel walls (named NCOFs-$NHNH_2$) are obtained *via* a post-synthetic modification strategy. Subsequently, the anticancer drug doxorubicin (DOX) as the model molecule is loaded through covalent linkage to yield NCOFs-NN-DOX. Finally, soybean phospholipid (SP) is coated on the surface of HNTs-NN-DOX, named NCOFs-NN-DOX@SP, to further enhance the dispersibility, stability and biocompatibility of HNTs in physiological solution. NCOFs-NN-DOX@SP showed an excellent and intelligent sustained-release effect with an almost sixfold increase at pH = 5.2 than at pH = 7.4. *In vitro* cell toxicity and imaging assays of NCOFs-NN-DOX@SP exhibited an enhanced therapeutic effect on Lewis lung carcinoma (LLC) cells, demonstrating that the fabricated NCOFs have a great potential in cancer therapy. Thus, this work provides a new way toward designing stimulus-responsive functionalized NCOFs and promotes their potential application as an on-demand drug delivery system in the field of cancer treatment.

Received 14th March 2024
Accepted 15th June 2024

DOI: 10.1039/d4ra01955e

rsc.li/rsc-advances

Introduction

Cancer is a malignant disease that seriously threatens human health.[1] However, traditional anti-cancer drugs have many limitations in cancer therapy, such as poor water-solubility, uncontrollable drug release, and lack of targeting, leading to severe side effects and reducing the survival rate of cancer patients.[2–4] Therefore, developing a cancer treatment method that improves drug delivery efficiency and reduces side effects is urgently needed.

Recently, more and more stimulus-responsive drug delivery nanosystems have received extensive attention from researchers for achieving effective drug release after tumor cell internalization. They reduce the side effects by capitalizing on some of the changes in biological stimuli that are unique to tumor pathology.[5–7] These stimulus-responsive systems have been investigated to control drug delivery in cancer treatments and include the following stimuli: (1) exogenous stimuli, such as light, thermos, ultrasound and electromagnetic fields, and (2) endogenous stimuli, such as enzymes stimuli and chemical stimuli.[8–13] As the typical chemical stimulus-responsive drug delivery system, pH-responsive drug delivery nanosystems have been employed extensively in cancer therapy.[9,14–16] The pH of the tumor extracellular environment is more acidic (pH 6.8) than that of the normal cells owing to the specific pathology of malignant tumors. In addition, the tumor extracellular environment of late endosomes and lysosomes is even more acidic, with much lower pH values (pH 5.4) than that of the normal tissue (pH 7.4).[17–20] Several acid-sensitive nanomaterials can be designed to achieve controlled drug release under the acidic conditions of the tumor, which is beneficial for improving therapeutic efficacy.[21–26] However, the anticancer drug delivery nanosystem with physical encapsulation presents premature drug leakage from the nanoplatform during the drug delivery process and leads to serious side effects.[27] Hence, the systems with pH-sensitive labile chemical bonds connecting drugs and

[a]*Department of Pharmacy, Hainan Women and Children's Medical Center, Haikou, Hainan, 570312, China*
[b]*Department of Pharmacy, Hainan General Hospital (Hainan Affiliated Hospital of Hainan Medical University), Haikou, Hainan, 570311, China*
[c]*Pharmaceutical and Bioengineering School, Hunan Chemical Vocational Technology College, Zhuzhou, 412006, China*
[d]*Department of Oncology, Hainan General Hospital (Hainan Affiliated Hospital of Hainan Medical University), Haikou, Hainan, 570311, China*
[e]*Department of Oncology, Hainan Cancer Hospital, Haikou, Hainan, 570312, China. E-mail: keyan634202863@126.com*

† Electronic supplementary information (ESI) available. See DOI: https://doi.org/10.1039/d4ra01955e

‡ These authors contributed equally to this work.

nanoparticles can be stable at normal physiological conditions, enabling the release of drugs under the acidic environments of tumor to achieve the controlled release of the anticancer drug temporally, spatially, and at the correct dosages.

Nanoscale covalent organic frameworks (NCOFs) are a recent new class of pure organic crystalline porous polymers materials using organic monomers with specific geometric shapes through dynamic covalent bonds. COFs were developed for the first time by Yaghi *et al.* in 2005. After that, a variety of COFs were developed.[28] As crystalline porous nanomaterials, NCOFs as new drug carriers have been used for cancer therapy due to their high porosity, high surface areas, functional groups of their surface pores, high stability, high biocompatibility and low physiological toxicity. These obvious benefits provide broad bio-application prospects for NCOFs in the field of drug delivery. However, there are still some limitations for NCOFs, such as poor hydrophilicity, dispersibility and biocompatibility.[29,30] Therefore, the *in situ* synthesis and post-synthesis modifications of NCOFs to introduce additional functionality will gain increasingly more attention in drug delivery. Unfortunately, achieving multifunctional NCOFs by *in situ* synthesis method is challenging as functional groups can interfere with the π–π interactions, which compromises the framework topological structure and integrity. By contrast, post-synthesis modifications achieve the controlled introduction of a greater variety of active units, such as metals, nanoparticles and functional groups, into the materials as needed under the premise of ensuring the integrity of the frame and crystalline structure. Thus, the exploration of more effective controlled drug release methods and enhancement of the biocompatibility and antitumor effect are of great significance to NCOFs, which deserve further research.

In this study, we report a nanoscale COFS (NCOFs)-based pH-sensitive drug delivery nanosystem (denoted as NCOFs-NN-DOX@SP) for tumor-triggered intracellular drug release. As shown in Scheme 1, sub-100 nm diameter crystalline NCOFs with relatively narrow size distribution were prepared according to the previous reported method. Then, the terephthalic dihydrazide group was covalently grafted onto the aldehyde group of NCOFs to form NCOFs-NHNH$_2$ *via* post-synthetic modification, which facilitated further biofunctionalization. Doxorubicin hydrochloride (DOX), as a small molecule model antitumor

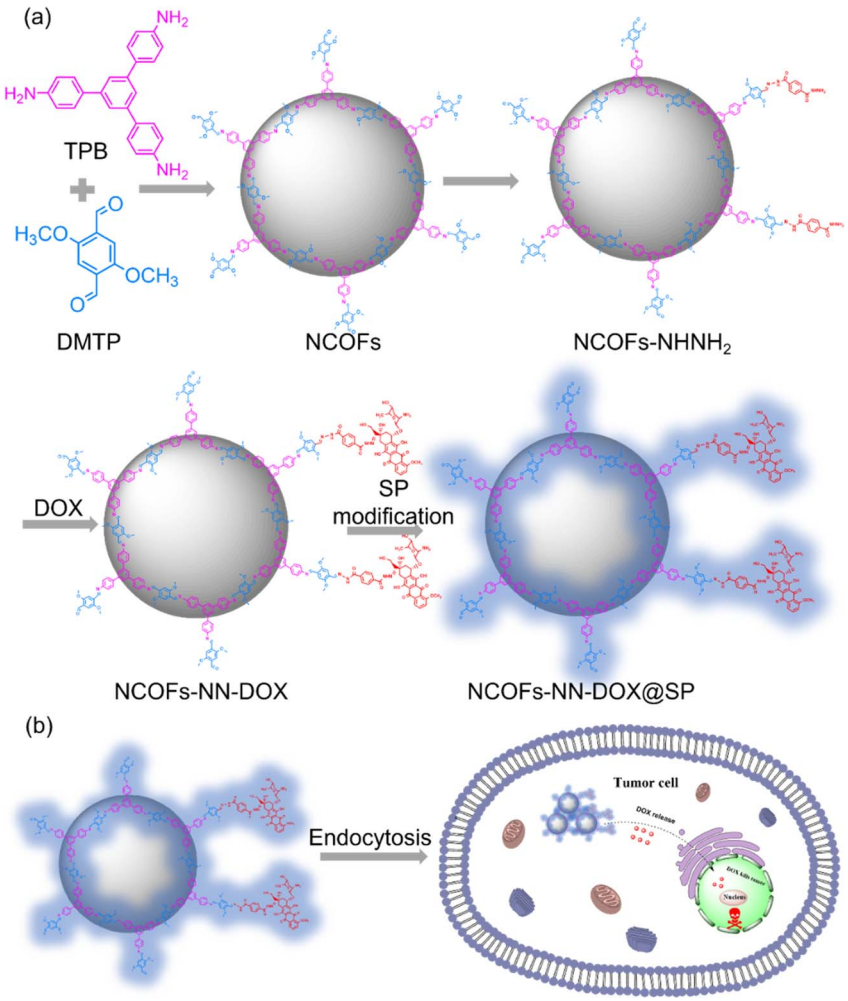

Scheme 1 (a) A schematic illustration of the preparation process of NCOFs-NN-DOX@SP. (b) The tumor-triggered intracellular drug release process of NCOFs-NN-DOX@SP.

drug, was grafted with NCOFs-$NHNH_2$ through an acid-labile hydrazone bond (NCOFs-NN-DOX) to prevent premature DOX release in the bloodstream and normal tissues before reaching the tumor tissues. As a control, DOX was loaded into NCOFs by the physical absorption method, named NCOFs @DOX (physical absorption). Finally, soybean phospholipid (SP) was anchored onto the surface of NCOFs-NN-DOX to increase the stability and hemocompatibility in body fluids, yielding NCOFs-NN-DOX@SP. The prepared NCOFs-NN-DOX@SP was characterized using various spectrometric methods, including powder X-ray diffraction (PXRD), Fourier transform infrared (FT-IR), scanning electron microscopy (SEM) and transmission electron microscopy (TEM). The drug release of NCOFs-NN-DOX@SP was pH-responsive, and the releasing efficiency was up to 84.7% at a pH value of 5.2. Furthermore, *in vitro* cytotoxicity was carried out to assess the ability to suppress Lewis lung carcinoma (LLC) cells of the NCOFs-NN-DOX@SP. The uptake effect of NCOFs-NN-DOX@SP on LLC was verified by endocytosis experiment. This work was aimed at constructing a new strategy on NCOFs as a novel pH-responsive carrier for delivery systems used in chemotherapy.

Experimental section

Materials

1,3,5-Tris(4-aminophenyl)-benzene (TPB, 98%), acetonitrile, 2,5-dimethoxyterephthaldehyde (DMTP, 98%), triethylamine (98%), acetic acid glacial (99%), 1,2-dichloroethane (DCM, 99%) and terephthalohydrazide (TD, 98%) were obtained from Shanghai Titan Scientific Co., Ltd (Shanghai, China). Soybean phospholipid (SP) and doxorubicin hydrochloride (98%) were purchased from Macklin (Shanghai, China). Dulbecco's modified Eagle's medium (DMEM) and fetal bovine serum (FBS) were obtained from Gibco. CCK-8 cell viability assay and 4′,6-diamidino-2-phenylindole dihydrochloride (DAPI) were purchased from Sigma-Aldrich. The Lewis lung carcinoma (LLC) cells were purchased from the Cell Bank of Shanghai Institutes for Biological Sciences (Shanghai, China).

Instruments

The scan electron microscopy (SEM) system (Hitachi S-4800, Hitachi, Japan) and transmission electron microscopy (TEM) measurements (JEM-2100) were used to observe the morphologies of the as-prepared NCOFs, NCOFs-$NHNH_2$, NCOFs-NN-DOX and NCOFs-NN-DOX@SP. Powder X-ray diffraction patterns (PXRD) were determined using a Bruker D8 Quest diffractometer in the range of 10–80° with Ni-filtered Cu/K-α radiation (1.5418 Å). Fourier translation infrared (FT-IR) spectra were obtained on a PerkinElmer Spectrum 100 spectrometer (PerkinElmer) using the KBr pellet method. Fluorescence experiments were carried out in a Gangdong F-320 fluorescence spectrophotometer at an excitation wavelength of $\lambda_{exc} = 480$ nm. The UV-visible spectra of all samples were obtained using a Shimadzu UV-3600 spectrophotometer. The dynamic light scattering and zeta potential test were recorded on a Malvern Zetasizer Nano ZS90.

Syntheses method

Synthesis of NCOFs. The synthesis of NCOFs was based on a literature reported method.[31] Briefly, a mixture of TPB (98.4 mg, 0.28 mmol), was dissolved in acetonitrile (1000 mL), then 2,5-dimethoxyterephthaldehyde (85.4 mg, 0.44 mmol), PVP-K30 (100 mg) and glacial acetic acid (5 mL) were added dropwise, respectively. The mixture was stirred at 25 °C for 12 h. The powder was collected by centrifugation and washed with acetonitrile five times to generate NCOFs as a yellow powder.

Synthesis of NCOFs-$NHNH_2$. A mixture of newly prepared NCOFs (100 mg), TD (194 mg, 1 mmol) and acetic acid glacial (10 mL, 3 M) were added to acetonitrile (100 mL), and stirred at 90 °C for 12 h. The reaction solution was cooled to room temperature. Subsequently, the powder was collected by centrifugation and washed with acetonitrile until the supernatant liquid was colorless to generate NCOFs-$NHNH_2$.

Synthesis of DOX-loaded NCOFs-$NHNH_2$ (covalent bond) and NCOFs (physical absorption). A 10 mg sample of NCOFs (physical absorption) and NCOFs-$NHNH_2$ (covalent bond) was added to 3 mL of a 1 mg mL^{-1} aqueous DOX-HCl solution, and stirred for 48 h at 50 °C in the dark, respectively. After cooling down, the final product was washed several times with doubly-distilled deionized water by centrifugation to remove the unloaded free DOX. The amount of DOX loaded in the NCOFs and NCOFs-$NHNH_2$ was calculated by UV-vis spectra using the following equations:

Loading capacity (LC) % = (Mass of loaded DOX in NPs/Total mass of NPs and loaded DOX) × 100%

Encapsulation efficiency (EE) % = (Mass of loaded DOX in NPs/Total mass of feeding drug) × 100%

Synthesis of NCOFs-NN-DOX@SP/NCOFs@DOX@SP. Soybean phospholipid (SP, 50 mg) was added to DCM (10 mL) to obtain a SP solution. The NCOFs-NN-DOX/NCOFs@DOX (10 mg) was dispersed in the above SP solution, and stirred at 25 °C overnight. Then, the NPs were collected by centrifugation. Finally, the product was washed with DCM five times and phosphate buffer saline (PBS) three times to remove the free SP.

Release of DOX from NCOFs-NN-DOX@SP/NCOFs@DOX@SP. The real-time drug release profile of DOX from NCOFs-NN-DOX@SP/NCOFs@DOX@SP was determined in PBS with acetate buffer (pH = 5.2) and phosphate buffer (pH = 7.4), respectively. 10 mg of NCOFs-NN-DOX@SP/NCOFs@DOX@SP was dispersed in 10 mL PBS, and then the mixture was stirred in the above buffer and shaken at 200 rpm in the dark. Aliquots containing 1 mL of suspension were separately taken at time intervals of 1, 2, 4, 6, 8, 12, 24, 36 and 48 h, and centrifuged to obtain the supernatant. The final cumulative release rate was obtained with the external standard method by the UV-vis absorbance of DOX at 480 nm in the supernatant. The experiment was repeated in triplicate.

Cell culture

Lewis lung carcinoma (LLC) cells were cultured in Dulbecco's Modified Eagle Medium (DMEM), supplemented with 10% fetal bovine serum (FBS), 100 U mL penicillin G sodium, and 100 μg

mL^{-1} streptomycin sulfate. The cells were cultured in an incubator containing 5% CO_2 at 37 °C.

Cytotoxicity assay

The cytotoxicities of free DOX, NCOFs and NCOFs-NN-DOX@SP were evaluated using a CCK-8 assay. Briefly, LLC were placed in a 96-well plate with a density at 1×10^4 cells per well, and incubated in DMEM for 24 h. The original medium was then sucked out, and the new medium containing different concentrations of free DOX and NCOFs-NN-DOX@SP (DOX concentrations of 1.25, 2.5, 5, 10, 20, 40 μg mL^{-1}) was added again. Similarly, the LLC also were incubated for 24 h with different concentrations of NCOFs (0–600 μg mL^{-1}). After the cells were incubated for another 24 h, the medium inside was again discarded, the cells were washed thrice with PBS and resuspended with fresh DMEM containing 10 μL of the 10% CCK-8 solution. After placing the plates in the dark at 37 °C for 3 h, the absorption value of each well was measured at 480 nm using a microplate reader.

Cell imaging

The cellular uptake capacity of NCOFs-NN-DOX@SP was investigated by fluorescent microscope using LLC. First, LLC (3×10^5 cells per well) were seeded in 6-well plates and incubated 24 h at 37 °C. Then, free DOX and NCOFs-NN-DOX@SP with 10 μg mL^{-1} DOX and 100 μg mL^{-1} of NCOFs were added. After different incubation times (0.5, 2 and 4 h), LLC were combined with 4% paraformaldehyde and fixed at room temperature for 15 min after washing with PBS three times. Then, the cells were washed with PBS five times and stained with DAPI dye. After washing with PBS for another five times, the DOX fluorescence was observed using a CLSM (ZEISS LSM780, Germany).

Results and discussion

Synthesis and characterization of NCOFs-NN-DOX@SP

In this study, the synthetic process of the pH-sensitive DOX loaded drug delivery nanosystem named NCOFs-NN-DOX@SP is summarized in Scheme 1. Firstly, NCOFs were synthesized by an imine condensation reaction between two tridentate building blocks, 1,3,5-tris(4-aminophenyl)-benzene (TPB) and acetonitrile, 2,5-dimethoxyterephthaldehyde (DMTP) under mild reaction conditions (CH_3CN, 25 °C, 12 h) with the aid of glacial acetic acid and PVP. NCOFs-$NHNH_2$ was prepared *via* Schiff-base condensation between the free end aldehyde groups on NCOFs and the monoamino-decorated terephthalohydrazide (TD) in acetonitrile under reflux for 12 h. NCOFs-$NHNH_2$ was further conjugated to DOX covalently through the acid-labile hydrazone bond in aqueous media, resulting in NCOFs-NN-DOX. Finally, SP was modified on the surface of NCOFs-NN-DOX to obtain NCOFs-NN-DOX@SP, which increased the biocompatibility and stability of the system. The encapsulated DOX was slowly released from the NCOFs nanocarrier with the degradation of the SP coating through a series of complicated chemical changes in the cancer cells.

Scanning electron microscopy (SEM) and transmission electron microscopy (TEM) showed that the as-synthesized NCOFs, NCOFs-$NHNH_2$, NCOFs-NN-DOX and NCOFs-NN-DOX@SP were obtained as radial spherical nanoparticles with diameters of ~160 nm (Fig. 1a–h), indicating that the TD and SP surface modification processes did not change their particle size and morphology. After being decorated by SP *via* the mixing process, there was a pale shell formed on the outer surface of the NCOFs-NN-DOX nanoparticles and the final material was named as NCOFs-NN-DOX@SP (Fig. 1h). It is well-known that the synthesis of well-dispersed nanoparticles, preferably in the size range 50–200 nm, is pivotal to access to better transport capacity, distribution and blood circulation *in vivo*. The SEM image shows that no significant difference of morphology was found in NCOFs before and after modification.

The crystallinity of NCOFs was first demonstrated using powder X-ray diffraction (PXRD) analysis with Cu Kα radiation. As exhibited in Fig. 1i, NCOFs also exhibited one well-defined peak observed at 2.85°, along with four less intense diffraction peaks at $2\theta = 4.82°$, 5.62°, 7.45° and 9.69°. These observed peaks were assigned to the (100), (110), (200), (210) and (220) facets, respectively. After loading with DOX and coating with SP, the diffraction pattern of NCOFs-NN-DOX@SP was masked to a certain degree, indicating that the framework structure maintained sufficient stability during functionalization. These results indicate that the crystalline of NCOFs was also preserved after introducing SP, indicating that the modified groups did not affect the structural integrity.

The groups and structure of NCOFs, NCOFs-$NHNH_2$, and NCOFs-NN-DOX were further characterized by Fourier transform infrared (FT-IR) spectroscopy, as shown in Fig. 1j and k. The peaks at 1671 and 3429 cm^{-1} associated with the free –CHO and $–NH_2$ groups in NCOFs directly evidenced the existence of bonding defects in the COFs.[32] The stretching vibration peaks of –C=N near 1619 cm^{-1} indicated that an imine linkage was present in NCOFs and NCOFs-$NHNH_2$. After being modified with TD, three new peaks at 3310, 1618 and 1340 cm^{-1} appeared, which belong to the stretching vibrations of –CO–NH, –C–N–N and –C–N, respectively. This proved that the Por species was grafted on NCOFs-$NHNH_2$. As shown in Fig. 1k, the new absorption peak at 1576 cm^{-1} was the C=C stretching vibration band of the aromatic ring on DOX, suggesting that DOX was covalently bonded to the framework *via* hydrazone reaction. All results indicated that the NCOFs-NN-DOX nanoparticles were synthesized successfully.

In addition, the surface charge and hydrodynamic diameter of NCOFs-based nanoparticles were measured in water by zeta potential measurement and dynamic light scattering (DLS). Fig. 2a illustrates that the hydrodynamic diameter of NCOFs-NN-DOX@SP was measured to be 195 nm, which is much large than those of NCOFs (165 nm), NCOFs-$NHNH_2$ (177 nm) and NCOFs-NN-DOX (180 nm). This confirms that SP was coated on NCOFs. It is well-known that NCOFs particles with sizes of lower than 200 nm can show better transport capacity, distribution and circulation *in vivo*. Therefore, most anticancer nanomedicines are applied intravenously and achieve their effects through passive targeting, which relies on non-specific

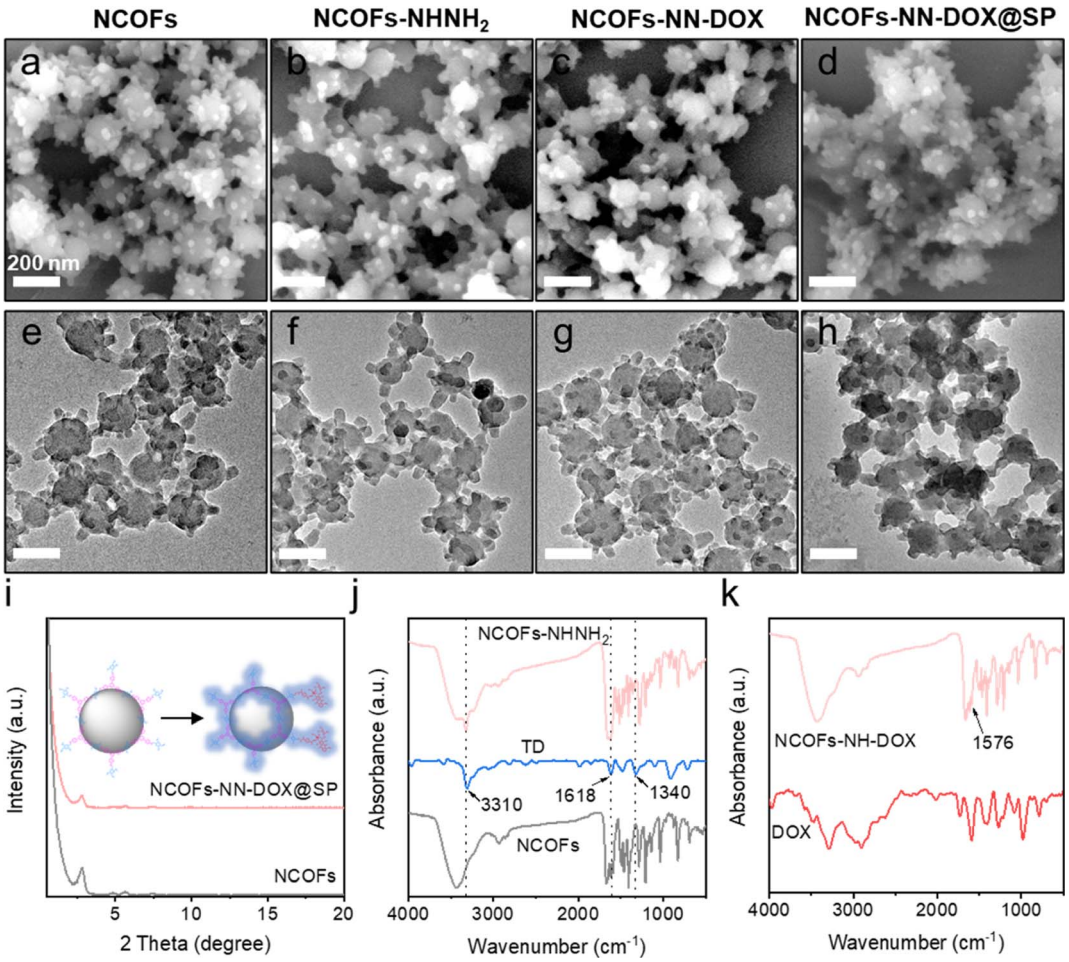

Fig. 1 SEM images and TEM images of (a and e) NCOFs, (b and f) NCOFs-$NHNH_2$, (c and g) NCOFs-NN-DOX, (d and h) NCOFs-NN-DOX@SP; (i) PXRD patterns of NCOFs and NCOFs-NN-DOX@SP; (j) FTIR spectra of terephthalohydrazide (TD), NCOFs, NCOFs-$NHNH_2$; (k) FTIR spectra of NCOFs-NN-DOX and DOX.

accumulation in tumor tissues. To investigate the intrinsic mechanism, the zeta potentials of different nanomaterials were characterized. As shown in Fig. 2b, the zeta potential for NCOFs was 16.5 mV and slightly increased to 21.5 mV for NCOFs-$NHNH_2$, confirming that TD was incorporated into NCOFs. Upon loading with DOX, the zeta potential of NCOFs-NN-DOX

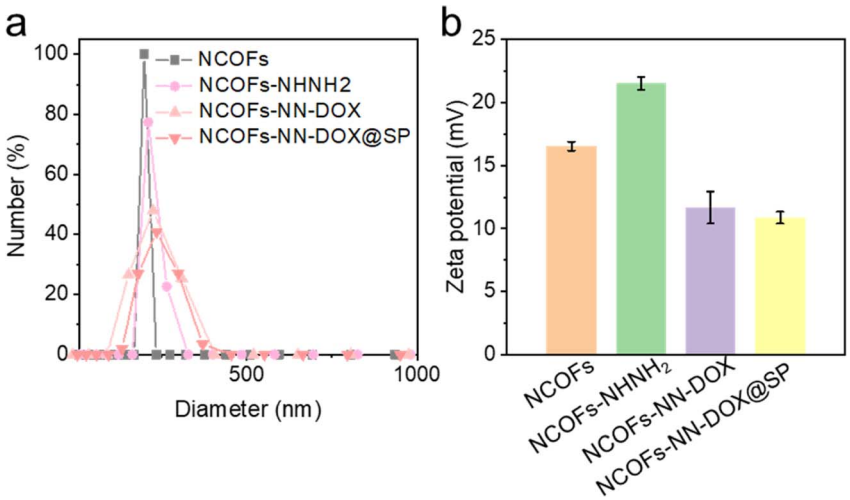

Fig. 2 (a) DLS result and (b) zeta potential result of NCOFs, NCOFs-$NHNH_2$, NCOFs-NN-DOX and NCOFs-NN-DOX@SP.

was observed to decrease to 11.7 mV, indicating the successful integration of DOX. After SP-functionalization, there was a significant change of the zeta potential to 10.8 mV (NCOFs-NN-DOX@SP). These results demonstrated that negatively charged SP was introduced as a layer for NCOFs-NN-DOX, and indicated the successful synthesis of the drug delivery system.

As shown in Fig. 3a, NCOFs-NN-DOX@SP showed good dispersibility, and NCOFs-NN-DOX@SP changed to a reddish color, indicating the successful loading of DOX. The drug-loaded NCOFs-NN-DOX@SP was investigated using UV-vis spectroscopy (Fig. 3b). The NCOFs showed an absorption peak at 470 nm, with a clear DOX peak observed at 486 nm after DOX loading. Thus, DOX absorbance in NCOFs-NN-DOX had shifted significantly, and this shift may be because of the covalent interactions between NCOFs and DOX molecules. Fig. 3c shows the photoluminescence spectra of NCOFs, free DOX and NCOFs-NN-DOX@SP. The fluorescence spectra showed that DOX has two fluorescence emission peaks at 553 nm and 580 nm after excitation with a 480 nm laser, and the emission peak location of DOX was not changed. It was also found that the NCOFs exhibited almost no fluorescence.

NCOFs were easily aggregated in physiological solutions because of the hydrophobicity of TPB and DMTP monomer. In order to address this issue, soybean phospholipid (SP) was further used to modify the surface of NCOFs-NN-DOX to endow the NCOFs-NN-DOX@SP with excellent stability and high dispersity in water, phosphate-buffered saline (PBS) and DMEM (containing 10% serum) medium. Fig. 3d shows that there was no apparent phenomena of agglomeration and sedimentation in these media at 37 °C for 48 h. Then, NCOFs-NN-DOX@SP was monitored by the DLS technique to examine the size distributions within 48 h in the same physiological conditions. We found that the sizes of NCOFs-NN-DOX@SP exhibited negligible fluctuations in these solutions throughout the 48 h measurement, indicating its excellent physiological stability (Fig. 3e). Such behavior indicated that NCOFs-NN-DOX@SP has an adequate circulation time period in the tumor microenvironment, which is highly suitable for biomedical applications.

Drug loading and release

The drug loading efficiency of NCOFs-$NHNH_2$ was investigated, and the results are shown in Fig. 4a. With the increasing concentration of the DOX: NCOFs-$NHNH_2$ mass ratio, the drug loading efficiency of the carrier gradually increases. When the mass ratio was up to 4, NCOFs-$NHNH_2$ entrapped DOX effectively with a loading efficiency of 41%, which was significantly higher than NCOFs, 30%. Compared with NCOFs without the hydrazone bond, the introduction of a large number of covalent bonds and the capillary action of the porous structure might play an important role in improving the drug loading of NCOFs-$NHNH_2$.

The release behaviors of NCOFs-NN-DOX@SP were investigated using PBS solutions with different pH values, such as tumor cell endosomes and lysosomes (pH = 4.5–5.2), tumor microenvironment (pH = 6.5–7.5) and human microenvironment including blood (pH = 7.3–7.4) at 37 °C. The DOX drug was loaded into NCOFs through physical absorption in the pores of NCOFs to yield NCOFs@DOX@SP. As shown in Fig. 4b,

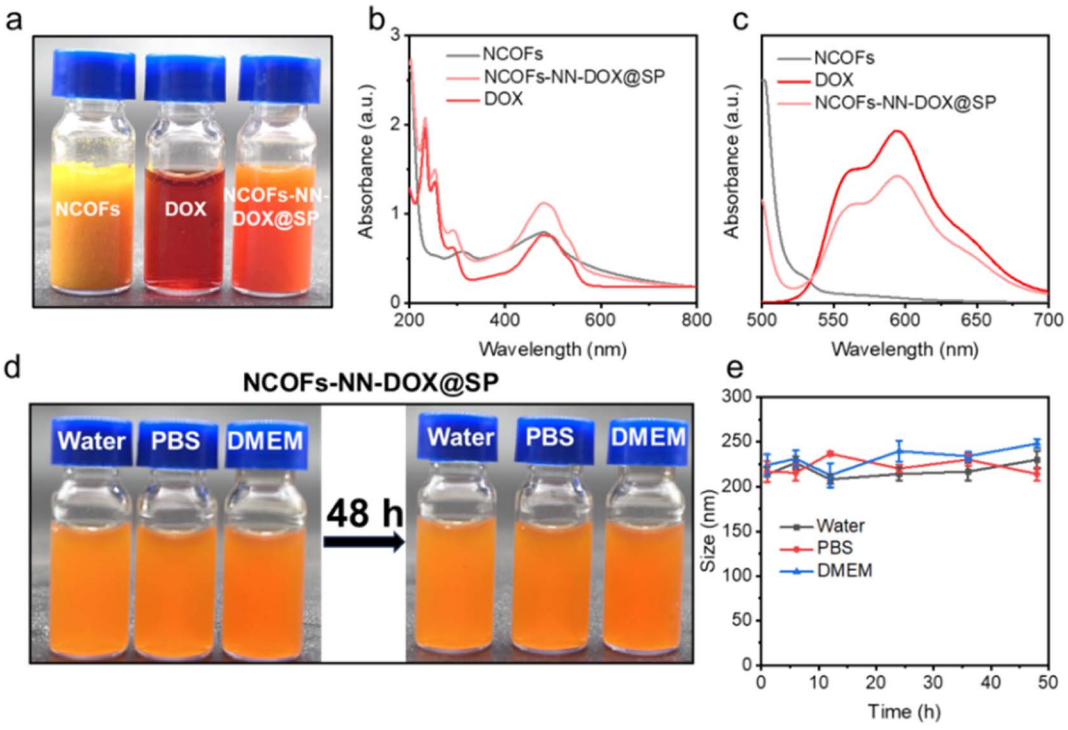

Fig. 3 (a) Photographs, (b) UV-vis absorption spectra and (c) fluorescence spectra of NCOFs, DOX and NCOFs-NN-DOX@SP. (d) Digital photographs and the changes of the hydrodynamic diameters of NCOFs-NN-DOX@SP dispersed in water, PBS and DMEM within 48 h.

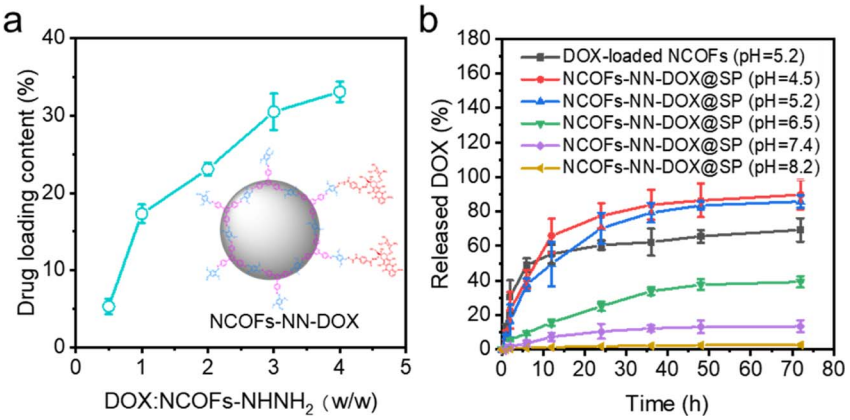

Fig. 4 (a) DOX loading capacity of the as-prepared NCOFs-$NHNH_2$; (b) DOX release at different pH conditions.

it is observed that the DOX release is relatively slow at a pH value of 7.4, and the cumulative release is 13.5% after 72 h. This is because NCOFs-NN-DOX@SP remains stable under a neutral environment, which prevents the premature release and reduces the side effect of DOX release to the normal cells and healthy tissues. When the pH was decreased to 6.5, the DOX release increases to 39.3%. About 85.7% of the DOX was released from the NCOFs-NN-DOX@SP at pH 5.2 in the tumor cell endosomes and lysosomes after 72 h. When the pH was 5.2, the cumulative release rate of HNTs-NN-DOX@SP was higher than that of NCOFs@DOX@SP (69.3%). HNTs-NN-DOX@SP was released very quickly (55.3%) before 12 h, and released almost completely. This is similar to the so-called burst release phenomenon of pure DOX.[33] When the incubation pH value was reduced to 4.5, a remarkable increase in DOX release was achieved with a high release percentage of 89.7% in 72 h. At alkaline pH condition (pH 8.2), the release behavior was notably depressed (only 2.7% after 72 h). When the pH decreases, the degradation of the hydrazone bonds of NCOFs-NN-DOX@SP in the acidic environment increases the release of the conjugated DOX. NCOFs-NN-DOX@SP could reduce the DOX release at extracellular physiological pH conditions, but significantly enhance DOX release at lysosome pH conditions. These results suggest that hydrazone-functionalized NCOFs-NN-DOX@SP has almost no off-target effect during anticancer drugs delivery. The above results can be accounted for by an explanation that the acid-labile covalent bond effectively improved the release effect of DOX drugs within the aqueous solution and debilitated the π–π interaction, electrostatic and hydrogen bonding between NCOFs and DOX.[34] Studies also show that DOX has a slightly higher solubility in an acidic environment that in a neutral solution, which also facilitates the DOX release. Therefore, the pH-responsive release characteristics and lasting release ability lead to NCOFs-NN-DOX@SP having high biosafety, which is important for further clinical translation and application in cancer therapy.

In vitro cell cytotoxicity

To evaluate the cytotoxicity of NCOFs, free DOX and NCOFs-NN-DOX@SP, an CCK-8 assay was conducted using Lewis lung carcinoma (LLC) cells (Fig. 5). Fig. 5a shows the survival rate of LLC, which was maintained at higher than 90.0% even after being incubated with a high concentration of 600 μg mL^{-1}. There was very little cytotoxicity and the cell viability was 97.8%, indicating the near absence of toxicity of NCOFs. The cytotoxic effects of free DOX and NCOFs-NN-DOX@SP at different

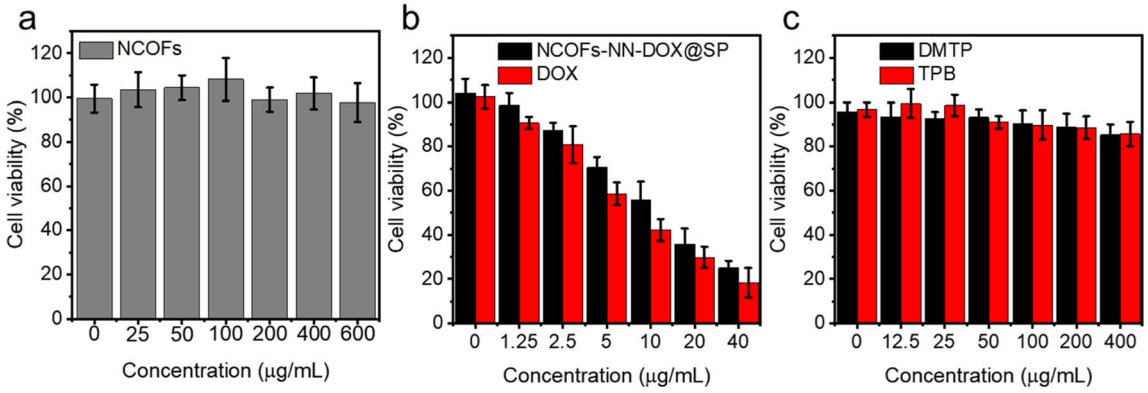

Fig. 5 Cell viability assay of (a) NCOFs, free DOX, (b) NCOFs-NN-DOX@SP, and (c) 2,5-dimethoxyterephthaldehyde (DMTP) and 1,3,5-tris(4-aminophenyl)-benzene (TPB) for 24 h.

concentrations on LLC cells after incubating for 24 h are shown in Fig. 5b. In the concentration range of 0–40.0 μg mL^{-1}, NCOFs-NN-DOX@SP showed a lower cytostatic rate compared with free DOX at each concentration. This might be due to the sustained release effect of NCOFs-NN-DOX@SP, which made the action concentration of DOX in NCOFs lower than that in free DOX group. Nonetheless, NCOFs-NN-DOX@SP still displayed obvious cytotoxicity at DOX concentrations of 40.0 μg mL^{-1} with the cell viability of 24.9%, indicating that NCOFs-NN-DOX@SP can release released DOX molecules effectively and have the potential to kill tumor cells under weakly acidic tumor microenvironments *in vitro*. There may be some impurities, including monomer of and 2, 5-dimethoxyterephthaldehyde (DMTP) and 1,3,5-tris(4-aminophenyl)-benzene (TPB) in the synthetic route of the NCOFs presented in the manuscript. Fig. 1J shows that after the reaction, the characteristic peaks of amino groups on TPB and the characteristic peaks of aldehyde groups on DMTP decreased in absorption. This indicated that the framework structure of NCOFs was obtained by forming imine bonds between the TPB monomer and DMTP monomer, which proved that there are no extra impurities in the NCOFs. Fig. 5c shows the cell viability after being incubated with TPB and DMTP for 24 h. For bare TPB and DMTP, there was no obvious cytotoxicity at concentrations of 0–400 μg mL^{-1}.

Cellular uptake of NCOFs-NN-DOX@SP *in vitro*

Based on the cytotoxicity findings, the cellular uptake and drug release of NCOFs-NN-DOX@SP were evaluated in LLC cells. As shown in Fig. S2,† when the cells were incubated with NCOFs and stained with DAPI, the control cells did not show any fluorescence during the 4 h of incubation. Notably, the NCOFs-NN-DOX@SP incubated cells exhibited time-dependent internalization of DOX. During the first 2 h, only weak DOX fluorescence was observed, but the DOX fluorescence was greatly increased with the incubation time. After 4 h, the incubated cells showed a strong DOX signal in the nucleus of the cells, indicating that the NCOFs-NN-DOX@SP system released DOX which was subsequently internalized in the nucleus (Fig. 6). Obviously, the responsive drug release characteristic should be attributed to the release of the hydrazone bond on NCOFs and the acidic cancer cell microenvironment in cancer cells. For free DOX, the red fluorescence was mainly concentrated in the nuclei, further confirming that DOX can quickly enter the nuclei to kill cancer cells (Fig. 7). This research indicated that NCOFs-NN-DOX@SP has the high potential for cancer cell-selective therapy.

In this work, hydrazone-decorated NCOFs as a pH-responsive doxorubicin (DOX) delivery system are designed *via* a post-synthetic modification strategy for efficient cancer therapy. The covalent organic frameworks (COFs) with pH-responsive drug delivery nanosystem mainly includes two synthesis strategies: (1) direct synthesis pH-responsive COFs by Schiff reaction between acidity activatable ligands, and (2) pH-responsive functions are introduced into COFs by post-synthetic modification. Comparatively, it offers a versatile avenue to introduce a greater variety of functional moieties into COFs without altering the structural regularity. More importantly, it avoids or minimizes the involvement of undesired side reactions during reticulation and functional incorporation. The functionalization of COFs *via* postsynthetic approach involves a specific bond formation, chemical reactions and host–guest interactions between the pendant groups or the active sites of

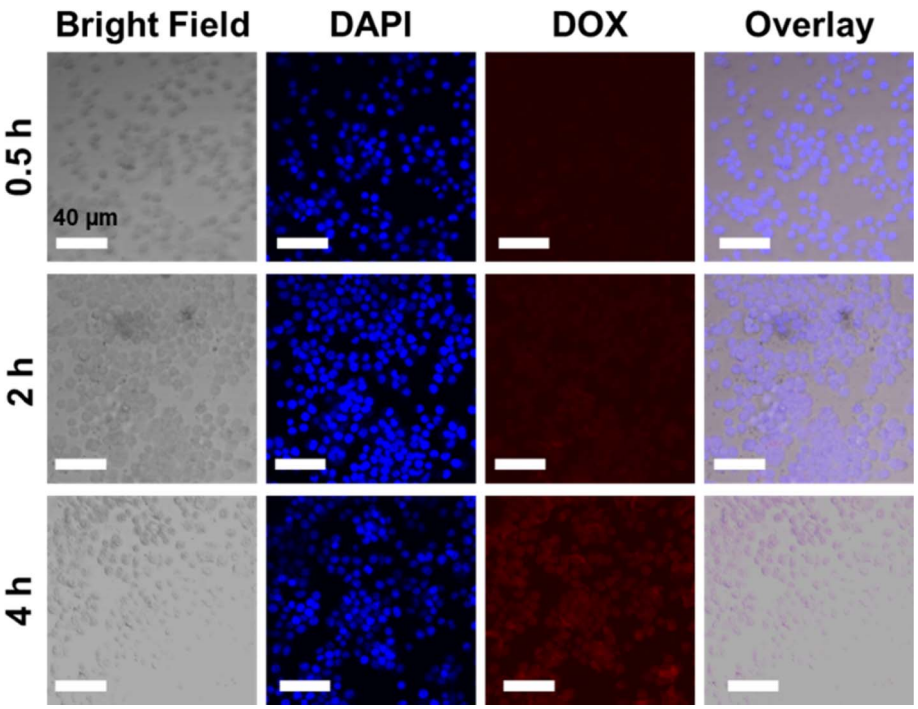

Fig. 6 Time-lapse image of NCOFs-NN-DOX@SP-incubated LLC cells. Red circles indicate aggregated NCOFs-NN-DOX@SP (scale bar: 40 μm).

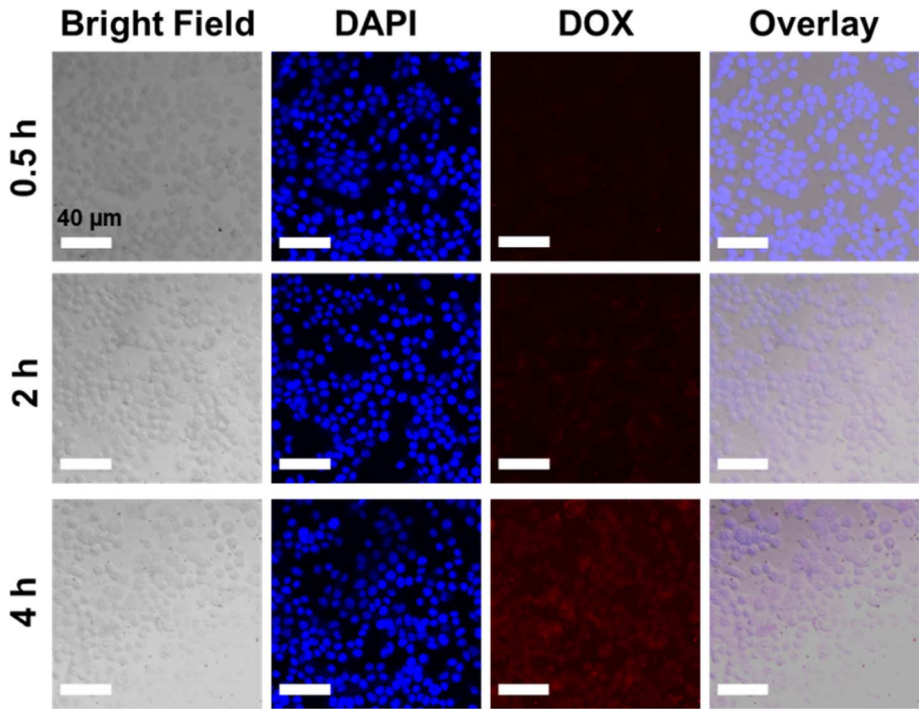

Fig. 7 Time-lapse image of free DOX-incubated LLC cells (scale bar: 40 μm).

the established COF and functional constituents. However, a critical challenge in the post-synthetic modification of COFs is the preservation of the basic framework structure of COFs during the modification process, especially under severe solvothermal and hydrothermal reaction conditions. A multistep-synthesis possibly introduces some toxic substances. Therefore, it is very significative work to explore a number of novel post-synthetic modification methods of COFs to control the release of anticancer drugs.

Conclusion

This work describes the first generalizable hydrazone group surface covalent approach for functionalizing the surface-exposed aldehyde group of NCOFs with a pH-responsive hydrazone bond. We anticipate that this method will find its use in the construction of many pH-responsive hydrazone-functionalized NCOFs drug delivery nanosystems. Firstly, NCOFs-NN-DOX was formed by the hydrazone bond terminal-functionalized NCOFs conjugated with doxorubicin with an acid-labile hydrazone bond, which have the capability of drug release in response to the tumor acidic environments and lysosome pH stimuli. Next, after coating with a SP shell, the as-obtained NCOFs-NN-DOX@SP exhibited the unique characteristics of pH-dependent drug release behavior and good biocompatibility. Furthermore, the cytotoxicity test indicated that NCOFs-NN-DOX@SP inhibited the viability and proliferation of LLC cells efficiently. In this work, the surface-exposed hydrazone bond of NCOFs not only serves as a pH-sensitive drug delivery nanosystem for DOX, but also includes any structural similarities drugs, such as epirubicin, valrubicin, alitretinoin, berubicin hydrochloride, and others. In total, this work opens a new surface modification strategy on COFs, and promotes their potential application as drug carriers in the field of cancer treatment.

Data availability

Data available on request from the authors.

Conflicts of interest

The authors declare no competing financial interests.

Acknowledgements

This project was supported by Hainan Province Clinical Medical Center (Grant No. QWYH202175), Health Research Project of Hainan Province (Grant No. 22A200100), Joint Project on Health Science and Technology Innovation of Hainan Province (Grant No. WSJK2024QN104), and The Education Department of Hainan Province (Grant No. Hnky2023-34).

References

1 R. L. Siegel, K. D. Miller and A. Jemal, *Ca-Cancer J. Clin.*, 2019, **69**, 7–34.
2 Z. Liu, K. Chen, C. Davis, S. Sherlock, Q. Cao, X. Chen and H. Dai, *Cancer Res.*, 2008, **68**, 6652–6660.
3 N. Muhammad, H. Zhao, W. Song, M. Gu, Q. Li, Y. Liu, C. Li, J. Wang and H. Zhan, *Nanotechnology*, 2021, **32**, 085105.

4 P. Smith, M. Choi, D. Charron, R. Ramesh and M. O'Reilly, *J. Acoust. Soc. Am.*, 2022, **151**, A152.
5 D. Gao, S. Asghar, R. Hu, S. Chen, R. Niu, J. Liu, Z. Chen and Y. Xiao, *Acta Pharm. Sin. B*, 2023, **13**, 1498–1521.
6 L. Luo, F. Xu, H. Peng, Y. Luo, X. Tian, G. Battaglia, H. Zhang, Q. Gong, Z. Gu and K. Luo, *J. Controlled Release*, 2020, **318**, 124–135.
7 S. Wang, W. Yang, J. Cui, X. Li, Y. Dou, L. Su, J. Chang, H. Wang, X. Li and B. Zhang, *Biomater. Sci.*, 2016, **4**, 338–345.
8 Y. Ju, Z. Wang, Z. Ali, H. Zhang, Y. Wang, N. Xu, H. Yin, F. Sheng and Y. Hou, *Nano Res.*, 2022, **15**, 4274–4284.
9 T. Li, D. Wang, Z. Guo, L. Lin, M. Meng, C. Liu, K. Hao, X. Pang, H. Tian and X. Chen, *Biomater. Sci.*, 2023, **11**, 6524–6536.
10 L. Ge, C. Qiao, Y. Tang, X. Zhang and X. Jiang, *Nano Lett.*, 2021, **21**, 3218–3224.
11 Y. Li, W. Chen, Y. Kang, X. Zhen, Z. Zhou, C. Liu, S. Chen, X. Huang, H.-J. Liu, S. Koo, N. Kong, X. Ji, T. Xie and W. Tao, *Nat. Commun.*, 2023, **14**, 6973.
12 W. Ou, S. Stewart, A. White, E. A. Kwizera, J. Xu, Y. Fang, J. G. Shamul, C. Xie, S. Nurudeen, N. P. Tirada, X. Lu, K. H. R. Tkaczuk and X. He, *Nat. Commun.*, 2023, **14**, 392.
13 Y. Li, W. Fan, X. Gu, S. Liu, T. He, S. Gou, W. Meng, M. Li, X. Liu, Y. Ren, C. Qi and K. Cai, *Adv. Funct. Mater.*, 2024, 2313540.
14 H. Ding, P. Tan, S. Fu, X. Tian, H. Zhang, X. Ma, Z. Gu and K. Luo, *J. Controlled Release*, 2022, **348**, 206–238.
15 Q. Sun, H. Bi, Z. Wang, C. Li, X. Wang, J. Xu, H. Zhu, R. Zhao, F. He, S. Gai and P. Yang, *Biomaterials*, 2019, **223**, 119473.
16 Q. Cao, Y. Zhang, Y. Tang, C. Wu, J. Wang and D. Li, *Sci. China: Chem.*, 2024, **67**, 1216–1223.
17 H. Zhu, J. Li, X. Qi, P. Chen and K. Pu, *Nano Lett.*, 2018, **18**, 586–594.
18 R. Mo and Z. Gu, *Mater. Today*, 2016, **19**, 274–283.
19 M. Wu, X. Niu, R. Zhang and Z. Ping Xu, *Adv. Drug Delivery Rev.*, 2022, **187**, 114360.
20 X. Jing, H. Hu, Y. Sun, B. Yu, H. Cong and Y. Shen, *Small Methods*, 2022, **6**, 2101437.
21 A. Grebinyk, S. Prylutska, S. Grebinyk, S. Ponomarenko, P. Virych, V. Chumachenko, N. Kutsevol, Y. Prylutskyy, U. Ritter and M. Frohme, *Nanoscale Adv.*, 2022, **4**, 5077–5088.
22 A. Abdollahy, M. Salehi, S. Mahami, A. Bernkop-Schnürch, H. Vahedi, A. M. Gharravi and M. Mehrabi, *Int. J. Pharm.*, 2024, **652**, 123838.
23 O. Osipova, N. Zakharova, I. Pyankov, A. Egorova, A. Kislova, A. Lavrentieva, A. Kiselev, T. Tennikova and E. Korzhikova-Vlakh, *J. Drug Delivery Sci. Technol.*, 2022, **69**, 103135.
24 W. Zhao, C. Yu, J. Zhao, F. Chen, X. Guan, H. Li, B. Tang, G. Yu, V. Valtchev, Y. Yan, S. Qiu and Q. Fang, *Small*, 2021, **17**, 2102630.
25 Y. Wang, X. Sun and Y. Wang, *RSC Adv.*, 2022, **12**, 16046–16050.
26 Y. Yang, Y. Liu, D. Tu, M. Chen, Y. Zhang, H. Gao and X. Chen, *Angew. Chem., Int. Ed.*, 2022, **61**, e202116983.
27 J. Yang, R. Zhang, F. Wang, J. Shang, S. Wu, Q. Ding, L. Yang, Q. Fan, Y. Ye and M. Zhou, *J. Drug Delivery Sci. Technol.*, 2023, **86**, 104693.
28 A. P. Côté, A. I. Benin, N. W. Ockwig, M. O'Keeffe, A. J. Matzger and O. M. Yaghi, *Science*, 2005, **310**, 1166–1170.
29 G. Zhang, X. Li, Q. Liao, Y. Liu, K. Xi, W. Huang and X. Jia, *Nat. Commun.*, 2018, **9**, 2785.
30 G. Zhang, Y. Ji, X. Li, X. Wang, M. Song, H. Gou, S. Gao and X. Jia, *Adv. Healthcare Mater.*, 2020, **9**, 2000221.
31 Q. Guan, L.-L. Zhou, Y.-A. Li, W.-Y. Li, S. Wang, C. Song and Y.-B. Dong, *ACS Nano*, 2019, **13**, 13304–13316.
32 L.-L. Zhou, Q. Guan, W. Zhou, J.-L. Kan, K. Teng, M. Hu and Y.-B. Dong, *ACS Nano*, 2023, **17**, 20445–20461.
33 G. Wang, D. Zhao, N. Li, X. Wang and Y. Ma, *J. Magn. Magn. Mater.*, 2018, **456**, 316–323.
34 J. Chai, Y. Ma, T. Guo, Y. He, G. Wang, F. Si, J. Geng, X. Qi, G. Chang, Z. Ren, R. Yu, L. Song and D. Li, *Appl. Clay Sci.*, 2022, **228**, 106630.